PROCEEDINGS OF SCIENCE

Multi-differential Jet Substructure Measurement in High Q^2 ep collisions with HERA-II Data

Vinicius Mikuni[a,*]

[a] *National Energy Research Scientific Computing Center, Berkeley Lab, Berkeley, CA 94720, USA*

E-mail: vmikuni@lbl.gov

The radiation pattern within quark- and gluon-initiated jets (jet substructure) is used extensively as a precision probe of the strong force as well as for optimizing event generators for nearly all tasks in high energy particle and nuclear physics. A detailed study of modern jet substructure observables, jet angularities, in electron-proton collisions is presented using data recorded using the H1 detector at HERA. The measurement is unbinned and multi-dimensional, using machine learning to correct for detector effects. Training these networks was enabled by the use of a large number of GPUs in the Perlmutter supercomputer at Berkeley Lab. The particle jets are reconstructed in the laboratory frame, using the k_{T} jet clustering algorithm. Results are reported at high transverse momentum transfer $Q^2 > 150$ GeV^2, and inelasticity $0.2 < y < 0.7$. The analysis is also performed in sub-regions of Q^2, thus probing scale dependencies of the substructure variables. The data are compared with a variety of predictions and point towards possible improvements of such models.

The European Physical Society Conference on High Energy Physics (EPS-HEP2023)
21-25 August 2023
Hamburg, Germany

*Speaker

PoS(EPS-HEP2023)231

Interactions between quarks and gluons (partons) are described by the theory of Quantum Chromodynamics (QCD) [1]. At high energy particle colliders, outgoing partons produce collimated sprays of particles known as jets. The radiation pattern inside jets (jet substructure) provides insight into the emergent properties of QCD at high energies.

Electron-proton collisions are ideal for studies of strong interaction processes. Jet properties were extensively studied at the HERA accelerator facility during data taking [2–5], but all of these studies pre-date modern jet substructure [6–10]. With new theoretical and methodological advances, novel insight can be extracted from from the preserved HERA data [11, 12] for precision QCD studies as well as for event generator improvements.

A canonical set of observables used to explore different aspects of the jet radiation pattern are the generalized angularities [13]:

$$\lambda_\beta^\kappa = \sum_{i \in \text{jet}} z_i^\kappa \left(\frac{R_i}{R_0}\right)^\beta, \tag{1}$$

with $z_i = p_{\text{T},i}/p_{\text{T}}^{\text{jet}}$ for a particle with momentum $p_{\text{T},i}$ transverse to the incoming beams clustered inside a jet with distance parameter R_0 and transverse momentum $p_{\text{T}}^{\text{jet}}$. The variable R_i is the Euclidean distance between particle i and the jet axis in the pseudorapidity-azimuthal angle plane.

These observables can be further augmented by multiplying the summand in Eq. 1 with the constituent electric charge q_i to form the charged-weighted angularities $\tilde{\lambda}_\beta^\kappa$.

In this work, normalized multi-differential cross sections are measured as a function of six jet angularities. The jets are selected at high transverse momenta in neutral current deep inelastic scattering (DIS) at high photon virtualities Q^2 , resulting in single jet events for the majority of the collisions.

The angularities include three infrared and collinear (IRC) unsafe distributions: the momentum dispersion $p_{\text{T}}\text{D} = \sqrt{\lambda_0^2}$ [14–16], the number of charged constituents $N_c = \tilde{\lambda}_0^0$, and the jet charge $Q_1 = \tilde{\lambda}_0^1$ [17, 18] as well as three IRC safe observables: the jet thrust (λ_2^1) [19], jet broadening (λ_1^1) [20–22], and an intermediate observable $\lambda_{1.5}^1$. Results are also reported as a function of the energy scale set by the DIS photon virtuality, thus probing the evolution of jet substructure.

New machine learning methods are used to simultaneously correct (unfold) all observables for detector effects, where graph neural networks are used for the first time to process all of the reconstructed particles inside jets. Making use of the unbinned nature of the data unfolding, both mean and standard deviation of all measured distributions are provided, after unfolding, at multiple Q^2 intervals, free of binning effects.

1. Experimental method

Results are reported using the data recorded by the H1 detector in the years 2006 and 2007 when protons and electrons/positrons (henceforth referred to as 'electrons') were collided at energies of 920 GeV and 27.6 GeV, respectively. The total integrated luminosity of this data sample corresponds to 228 pb^{-1} [23].

Events containing scattered electrons with energy $E_{e'} > 11$ GeV are kept for further analysis, resulting in a trigger efficiency higher than 99.5% [24, 25]. Backgrounds from additional

processes such as cosmic rays, beam-gas interactions, photoproduction, charged-current DIS and QED Compton processes are rejected after dedicated selection [25, 26], resulting in negligible background contamination.

The inelasticity and photon virtuality are reconstructed using the Σ method [27]. The hadronic final state (HFS) objects are reconstructed using the energy flow algorithm [28–30] after removing energy clusters and tracks associated to the electron. Additionally, events are required to have $45 < \Sigma_{\text{had}} + \Sigma_{e'} < 65$ GeV to suppress initial-state QED radiation and contributions from photoproduction.

Jets are defined in the laboratory frame by clustering HFS objects satisfying $-1.5 < \eta_{\text{lab}} < 2.75$. The FastJet 3.3.2 package [31, 32] is used with longitudinally invariant k_{T} clustering algorithm [33, 34] using the default E-scheme and distance parameter $R_0 = 1$. All jets in the event with $p_{\text{T}} > 5$ GeV are kept for further analysis. Reconstructed and generator level jets are matched by requiring the distance $\Delta R = \sqrt{(\phi^{\text{jet}}_{\text{gen}} - \phi^{\text{jet}}_{\text{reco}})^2 + (\eta^{\text{jet}}_{\text{gen}} - \eta^{\text{jet}}_{\text{reco}})^2} < 0.9$.

Results are presented after unfolding the data to particle level for events in the kinematic region defined by $Q^2 > 150$ GeV^2, $0.2 < y < 0.7$, $p^{\text{jet}}_{\text{T}} > 10$ GeV, and $-1.0 < \eta^{\text{jet}}_{\text{lab}} < 2.5$.

2. Monte Carlo simulations

Detector acceptance and resolution effects are estimated using Djangoh 1.4 [35] and Rapgap 3.1 [36] event generators. The CTEQ6L Parton distribution function (PDF) set [37] and the Lund hadronization model [38] with parameters determined by the ALEPH Collaboration [39] are used for the non-perturbative components. Each of these generators is combined with a detailed simulation of the H1 detector response based on the Geant3 simulation program [40] and reconstructed in the same way as data.

Additional predictions are made using a set of state-of-the-art generators developed mostly for pp collisions. Predictions from Pythia 8.3 [41, 42] are used for comparison using the default implementation and two additional parton shower implementations: Vincia [43, 44] and Dire [45]. The NNPDF3.1 PDF set [46] is used for both default and Vincia implementation and the MMHT14nlo68cl PDF set [47] is used for the Dire implementation. Predictions from Herwig 7.2 [48, 49] are calculated using the cluster hadronisation model [50] with default implementation parameters and alternative MatchBox [51] matching and merging [50] schemes. Predictions from the pre-release version of Sherpa 3.0 [52] are provided by the Sherpa authors featuring a new cluster hadronisation model [53] and matrix element calculation at next-to-leading order (NLO) obtained from OpenLoops with the Sherpa Dipole Shower [54] based on the truncated shower method [55, 56].

3. Unfolding methodology

The unfolding procedure is carried out by simultaneously unfolding the six jet angularities, jet momentum $(p_{\text{T}}, \eta, \phi)$, and photon virtuality Q^2 using the OmniFold method [57, 58].

Up to 30 HFS objects clustered inside jets are used as inputs to a graph neural network (GNN), where HFS objects are represented as nodes of the graph. These inputs are used only during the first step of the OmniFold algorithm. This novel hybrid approach has been found to reduce uncertainties by accounting for all possible covariates of the detector response.

For each HFS object with momentum (p_T,η,ϕ) and electric charge q, the kinematic information used for the first step classifier is the set (z,$\Delta\eta$,$\Delta\phi$,q), with $z = p_T/p_T^{jet}$, $\Delta\eta = \eta - \eta^{\text{jet}}$, and $\Delta\phi = \phi - \phi^{\text{jet}}$. Jet momentum ($p_T^{\text{jet}}$, η^{jet},ϕ^{jet}) and Q^2 information are also included in the aggregation function of the graph implementation. In total, $30 \times 4 + 4 = 124$ features are considered during this first step, requiring the network implementation to learn the differences between data and simulation in a high-dimensional setting.

The Point Cloud Transformer (PCT) [59, 60] GNN architecture is chosen to train the classifier. This GNN architecture learns the relationship between nearby particles through the use of attention layers, resulting in state-of-the-art classification performance for different types of jets [60]. The local neighborhood in PCT is defined by selecting the five closest neighbors of each particle with distances calculated in the $\eta - \phi$ plane. The impact of adding more than 30 particles was found to be negligible.

In the second step, a simplified classifier architecture is used. The inputs of the classifier are the same jet kinematic information and Q^2 used in the previous step, but HFS objects are replaced by the jet observables that are reported in the final results. This choice decreases the number of inputs by an order of magnitude and reduces the training time of the classifier by a factor five. To derive the unfolded results and uncertainties, 2800 neural networks are trained independently using 128 graphic processing units (GPUs) simultaneously with the Perlmutter supercomputer [61] and Horovod [62] library used for parallel distributed training.

4. Uncertainties

Systematic uncertainties on the reconstruction of the data observables are estimated by varying the relevant aspect of the simulation and carrying out the full unfolding procedure with the varied simulation set. Uncertainties on HFS objects include the energy scale from two different contributions: HFS objects contained in high p_T jets and other HFS objects. In both cases, the energy-scale uncertainty is ±1%. Both uncertainty sources are estimated separately [63, 64] by varying the corresponding HFS energy by ±1%. An uncertainty of ±20 mrad is assigned to the azimuthal angle determination of HFS objects. Lepton uncertainties are considered in the Q^2 determination and the uncertainty on the lepton energy scale ranges from ±0.5% to ±1% [64, 65]. Uncertainties on the azimuthal angle of the scattered lepton are estimated to be ±1 mrad [66].

Additional uncertainties from the unfolding procedure are estimated to cover a possible bias from the generator choice used to perform the unfolding procedure. A model uncertainty is estimated by unfolding the data with Djangoh instead of the default Rapgap. In addition, a non-closure uncertainty is estimated by unfolding Djangoh as pseudo-data using the Rapgap simulation and comparing to the Djangoh at particle level. The combined effect of the unfolding uncertainties are often below 10% in all distributions. The statistical uncertainty is estimated using the bootstrap technique [67]. The unfolding procedure is repeated on 100 pseudo datasets, each defined by resampling the original dataset with replacement.

5. Results

Unfolded results of the normalized differential particle level cross sections of the jet substructure observables are presented in Figs. 1 in the kinematic region described in Sec. 1. Unfolded distributions are shown in Fig. 1. Mean and standard deviation are calculated from the unbinned, unfolded event sample, and are shown for the six jet angularities in four Q^2 ranges in Figs. 2 and 3, respectively.

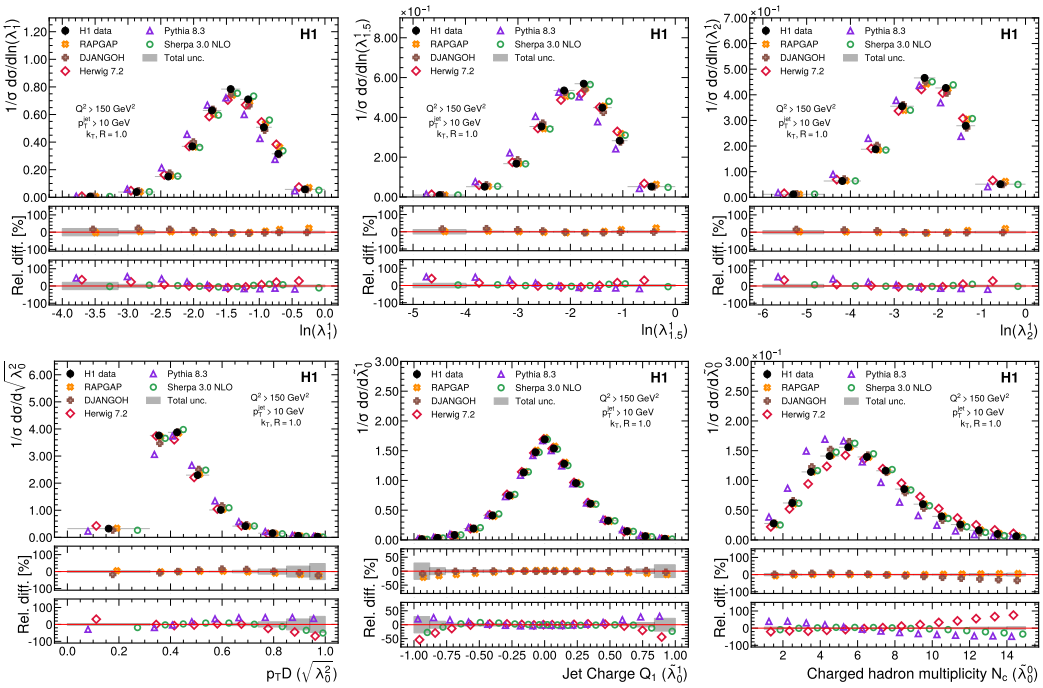

Figure 1: Measured cross sections, normalized to the inclusive jet production cross section as a function of the jet angularities measured in this work.

Predictions by the DIS MC generators, DJANGOH and RAPGAP, and by general purpose simulators, SHERPA, HERWIG, PYTHIA show a good agreement with data for most observables. RAPGAP shows a good agreement with data in all distributions and Q^2 intervals, while the DJANGOH generator shows worse agreement with data at high Q^2 values. General purpose simulators often show bigger discrepancies in the low Q^2 region.

6. Conclusion

A first measurement of jet angularities in neutral current DIS events with $Q^2 > 150$ GeV^2 and $0.2 < y < 0.7$, as well as divided into four Q^2 intervals is presented.

The process of unfolding detector effects made use of novel machine learning methods. All measured distributions are simultaneously unfolded using the OMNIFOLD approach. Kinematic information from each reconstructed particle clustered inside a jet is input to a dedicated graph neural network implementation that learns the correlation between particles clustered inside a jet. On particle level, however, the jet substructure is represented by the generalized angularities alone.

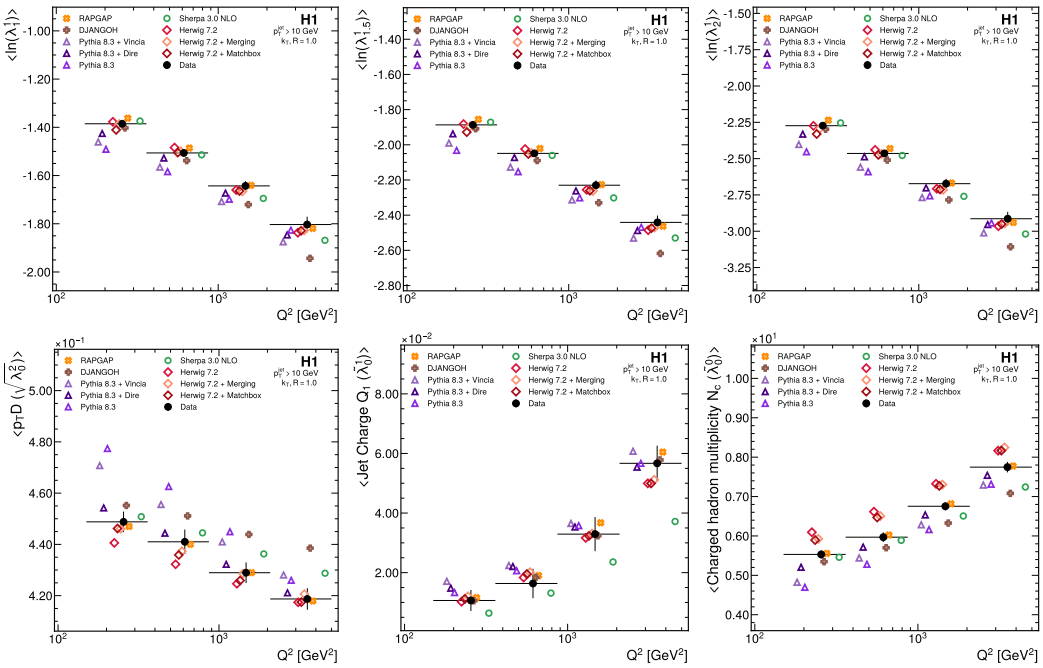

Figure 2: Measured mean of the unfolded jet observables for multiple Q^2 intervals reported in this work.

While the unfolding procedure is unbinned, results are provided as histograms for both single- and multi-differential cross sections to ease the comparison with different theory predictions. Mean and standard deviation of all observables are also calculated after unfolding. Theory predictions from dedicated DIS simulators provide an overall good description of all measured quantities. General purpose simulators are also able to describe the data well and show a good agreement with most of the jet angularities studied.

References

[1] F. Gross, et al., 50 Years of Quantum Chromodynamics (12 2022). arXiv:2212.11107.

[2] C. Adloff, et al., Measurement of internal jet structure in dijet production in deep inelastic scattering at HERA, Nucl. Phys. B 545 (1999) 3–20. arXiv:hep-ex/9901010, doi:10.1016/S0550-3213(99)00118-2.

[3] J. Breitweg, et al., Measurement of jet shapes in high Q^2 deep inelastic scattering at HERA, Eur. Phys. J. C 8 (1999) 367–380. arXiv:hep-ex/9804001, doi:10.1007/s100520050471.

[4] S. Chekanov, et al., Measurement of subjet multiplicities in neutral current deep inelastic scattering at HERA and determination of alpha(s), Phys. Lett. B 558 (2003) 41–58. arXiv:hep-ex/0212030, doi:10.1016/S0370-2693(03)00216-8.

[5] S. Chekanov, et al., Substructure dependence of jet cross sections at HERA and determination of alpha(s), Nucl. Phys. B 700 (2004) 3–50. arXiv:hep-ex/0405065, doi:10.1016/j.nuclphysb.2004.08.049.

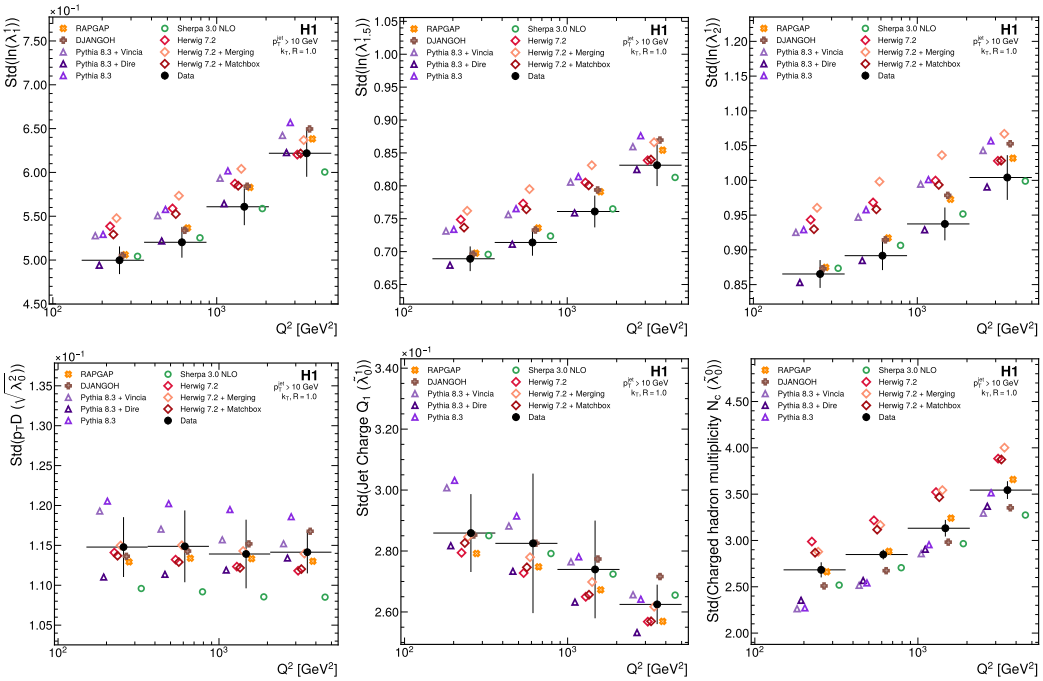

Figure 3: Measured standard deviation of the unfolded jet observables for multiple Q^2 intervals reported in this work.

[6] A. Altheimer, et al., Jet Substructure at the Tevatron and LHC: New results, new tools, new benchmarks, J. Phys. G 39 (2012) 063001. arXiv:1201.0008, doi:10.1088/0954-3899/39/6/063001.

[7] A. Altheimer, et al., Boosted Objects and Jet Substructure at the LHC. Report of BOOST2012, held at IFIC Valencia, 23rd-27th of July 2012, Eur. Phys. J. C 74 (3) (2014) 2792. arXiv:1311.2708, doi:10.1140/epjc/s10052-014-2792-8.

[8] D. Adams, et al., Towards an Understanding of the Correlations in Jet Substructure, Eur. Phys. J. C 75 (9) (2015) 409. arXiv:1504.00679, doi:10.1140/epjc/s10052-015-3587-2.

[9] R. Kogler, et al., Jet Substructure at the Large Hadron Collider: Experimental Review, Rev. Mod. Phys. 91 (4) (2019) 045003. arXiv:1803.06991, doi:10.1103/RevModPhys.91.045003.

[10] A. J. Larkoski, I. Moult, B. Nachman, Jet substructure at the large hadron collider: A review of recent advances in theory and machine learning, Physics Reports 841 (2020) 1–63, jet substructure at the Large Hadron Collider: A review of recent advances in theory and machine learning. doi:https://doi.org/10.1016/j.physrep.2019.11.001.
URL https://www.sciencedirect.com/science/article/pii/S0370157319303643

[11] D. M. South, M. Steder, The H1 Data Preservation Project, J. Phys. Conf. Ser. 396 (2012) 062019. arXiv:1206.5200, doi:10.1088/1742-6596/396/6/062019.

[12] D. Britzger, S. Levonian, S. Schmitt, D. South, Preservation through modernisation: The software of the H1 experiment at HERA, EPJ Web Conf. 251 (2021) 03004. arXiv:2106.11058, doi:10.1051/epjconf/202125103004.

[13] A. J. Larkoski, J. Thaler, W. J. Waalewijn, Gaining (Mutual) Information about Quark/Gluon Discrimination, JHEP 11 (2014) 129. arXiv:1408.3122, doi:10.1007/JHEP11(2014)129.

[14] S. Chatrchyan, et al., Search for a Higgs boson in the decay channel H to ZZ(*) to q qbar ℓ^- l+ in pp collisions at $\sqrt{s}$ = 7 TeV, JHEP 04 (2012) 036. arXiv:1202.1416, doi:10.1007/JHEP04(2012)036.

[15] F. Pandolfi, Search for the Standard Model Higgs Boson in the $H \to ZZ \to l^+l^-q\overline{q}$ Decay Channel at CMS, Ph.D. thesis, Zurich, ETH, New York (2012). doi:10.1007/978-3-319-00903-2.

[16] Pileup Jet Identification, Tech. rep., CERN, Geneva (2013).
URL https://cds.cern.ch/record/1581583

[17] R. D. Field, R. P. Feynman, A Parametrization of the Properties of Quark Jets, Nucl. Phys. B 136 (1978) 1. doi:10.1016/0550-3213(78)90015-9.

[18] D. Krohn, M. D. Schwartz, T. Lin, W. J. Waalewijn, Jet Charge at the LHC, Phys. Rev. Lett. 110 (21) (2013) 212001. arXiv:1209.2421, doi:10.1103/PhysRevLett.110.212001.

[19] E. Farhi, A QCD Test for Jets, Phys. Rev. Lett. 39 (1977) 1587–1588. doi:10.1103/PhysRevLett.39.1587.

[20] S. Catani, G. Turnock, B. R. Webber, Jet broadening measures in e^+e^- annihilation, Phys. Lett. B 295 (1992) 269–276. doi:10.1016/0370-2693(92)91565-Q.

[21] P. E. L. Rakow, B. R. Webber, Transverse Momentum Moments of Hadron Distributions in QCD Jets, Nucl. Phys. B 191 (1981) 63–74. doi:10.1016/0550-3213(81)90286-8.

[22] R. K. Ellis, B. R. Webber, QCD Jet Broadening in Hadron Hadron Collisions, Conf. Proc. C 860623 (1986) 74.

[23] F. D. Aaron, et al., Determination of the Integrated Luminosity at HERA using Elastic QED Compton Events, Eur. Phys. J. C 72 (2012) 2163, [Erratum: Eur.Phys.J.C 74, 2733 (2014)]. arXiv:1205.2448, doi:10.1140/epjc/s10052-012-2163-2.

[24] F. D. Aaron, et al., Inclusive Deep Inelastic Scattering at High Q^2 with Longitudinally Polarised Lepton Beams at HERA, JHEP 09 (2012) 061. arXiv:1206.7007, doi:10.1007/JHEP09(2012)061.

[25] V. Andreev, et al., Measurement of multijet production in ep collisions at high Q^2 and determination of the strong coupling α_s, Eur. Phys. J. C 75 (2) (2015) 65. arXiv:1406.4709, doi:10.1140/epjc/s10052-014-3223-6.

[26] V. Andreev, et al., Measurement of Jet Production Cross Sections in Deep-inelastic ep Scattering at HERA, Eur. Phys. J. C 77 (4) (2017) 215, [Erratum: Eur.Phys.J.C 81, 739 (2021)]. arXiv:1611.03421, doi:10.1140/epjc/s10052-017-4717-9.

[27] U. Bassler, G. Bernardi, On the kinematic reconstruction of deep inelastic scattering at HERA: The Sigma method, Nucl. Instrum. Meth. A 361 (1995) 197–208. arXiv:hep-ex/9412004, doi:10.1016/0168-9002(95)00173-5.

[28] M. Peez, Search for deviations from the standard model in high transverse energy processes at the electron proton collider HERA, Other thesis (10 2003). doi:10.3204/DESY-THESIS-2003-023.

[29] S. Hellwig, Untersuchung der $D^* - \pi_{slow}$ Double Tagging Methode in Charmanalysen, Master's thesis, Hamburg U. (2004).

[30] B. Portheault, First measurement of charged and neutral current cross sections with the polarized positron beam at HERA II and QCD-electroweak analyses, Other thesis (3 2005).

[31] M. Cacciari, G. P. Salam, G. Soyez, FastJet User Manual, Eur. Phys. J. C 72 (2012) 1896. arXiv:1111.6097, doi:10.1140/epjc/s10052-012-1896-2.

[32] M. Cacciari, G. P. Salam, Dispelling the N^3 myth for the k_t jet-finder, Phys. Lett. B 641 (2006) 57–61. arXiv:hep-ph/0512210, doi:10.1016/j.physletb.2006.08.037.

[33] S. Catani, Y. L. Dokshitzer, M. H. Seymour, B. R. Webber, Longitudinally invariant K_t clustering algorithms for hadron hadron collisions, Nucl. Phys. B 406 (1993) 187–224. doi:10.1016/0550-3213(93)90166-M.

[34] S. D. Ellis, D. E. Soper, Successive combination jet algorithm for hadron collisions, Phys. Rev. D 48 (1993) 3160–3166. arXiv:hep-ph/9305266, doi:10.1103/PhysRevD.48.3160.

[35] K. Charchula, G. A. Schuler, H. Spiesberger, Combined QED and QCD radiative effects in deep inelastic lepton - proton scattering: The Monte Carlo generator DJANGO6, Comput. Phys. Commun. 81 (1994) 381–402. doi:10.1016/0010-4655(94)90086-8.

[36] H. Jung, Hard diffractive scattering in high-energy e p collisions and the Monte Carlo generator RAPGAP, Comput. Phys. Commun. 86 (1995) 147–161. doi:10.1016/0010-4655(94)00150-Z.

[37] J. Pumplin, D. R. Stump, J. Huston, H. L. Lai, P. M. Nadolsky, W. K. Tung, New generation of parton distributions with uncertainties from global QCD analysis, JHEP 07 (2002) 012. arXiv:hep-ph/0201195, doi:10.1088/1126-6708/2002/07/012.

[38] B. "Andersson, G. Gustafson, G. Ingelman, T. Sjöstrand, Parton Fragmentation and String Dynamics, Phys. Rept. 97 (1983) 31–145. doi:10.1016/0370-1573(83)90080-7.

[39] S. Schael, et al., Bose-Einstein correlations in W-pair decays with an event-mixing technique, Phys. Lett. B 606 (2005) 265–275. doi:10.1016/j.physletb.2004.12.018.

[40] R. Brun, F. Bruyant, M. Maire, A. C. McPherson, P. Zanarini, GEANT3 (9 1987).

[41] T. Sjöstrand, S. Mrenna, P. Z. Skands, PYTHIA 6.4 Physics and Manual, JHEP 05 (2006) 026. arXiv:hep-ph/0603175, doi:10.1088/1126-6708/2006/05/026.

[42] T. Sjöstrand, S. Ask, J. R. Christiansen, R. Corke, N. Desai, P. Ilten, S. Mrenna, S. Prestel, C. O. Rasmussen, P. Z. Skands, An introduction to PYTHIA 8.2, Comput. Phys. Commun. 191 (2015) 159–177. arXiv:1410.3012, doi:10.1016/j.cpc.2015.01.024.

[43] W. T. Giele, D. A. Kosower, P. Z. Skands, A simple shower and matching algorithm, Phys. Rev. D 78 (2008) 014026. arXiv:0707.3652, doi:10.1103/PhysRevD.78.014026.

[44] W. T. Giele, L. Hartgring, D. A. Kosower, E. Laenen, A. J. Larkoski, J. J. Lopez-Villarejo, M. Ritzmann, P. Skands, The VINCIA Parton Shower, PoS DIS2013 (2013) 165. arXiv:1307.1060, doi:10.22323/1.191.0165.

[45] S. Höche, S. Prestel, The midpoint between dipole and parton showers, Eur. Phys. J. C 75 (9) (2015) 461. arXiv:1506.05057, doi:10.1140/epjc/s10052-015-3684-2.

[46] R. D. Ball, et al., Parton distributions from high-precision collider data, Eur. Phys. J. C 77 (10) (2017) 663. arXiv:1706.00428, doi:10.1140/epjc/s10052-017-5199-5.

[47] L. A. Harland-Lang, A. D. Martin, P. Motylinski, R. S. Thorne, Parton distributions in the LHC era: MMHT 2014 PDFs, Eur. Phys. J. C 75 (5) (2015) 204. arXiv:1412.3989, doi:10.1140/epjc/s10052-015-3397-6.

[48] J. Bellm, et al., Herwig 7.0/Herwig++ 3.0 release note, Eur. Phys. J. C 76 (4) (2016) 196. arXiv:1512.01178, doi:10.1140/epjc/s10052-016-4018-8.

[49] M. Bahr, et al., Herwig++ Physics and Manual, Eur. Phys. J. C 58 (2008) 639–707. arXiv:0803.0883, doi:10.1140/epjc/s10052-008-0798-9.

[50] J. Bellm, et al., Herwig 7.2 release note, Eur. Phys. J. C 80 (5) (2020) 452. arXiv:1912.06509, doi:10.1140/epjc/s10052-020-8011-x.

[51] L. Lönnblad, S. Prestel, Merging Multi-leg NLO Matrix Elements with Parton Showers, JHEP 03 (2013) 166. arXiv:1211.7278, doi:10.1007/JHEP03(2013)166.

[52] E. Bothmann, et al., Event Generation with Sherpa 2.2, SciPost Phys. 7 (3) (2019) 034. arXiv:1905.09127, doi:10.21468/SciPostPhys.7.3.034.

[53] G. S. Chahal, F. Krauss, Cluster Hadronisation in Sherpa, SciPost Phys. 13 (2) (2022) 019. arXiv:2203.11385, doi:10.21468/SciPostPhys.13.2.019.

[54] S. Schumann, F. Krauss, A Parton shower algorithm based on Catani-Seymour dipole factorisation, JHEP 03 (2008) 038. arXiv:0709.1027, doi:10.1088/1126-6708/2008/03/038.

[55] S. "Höche, F. Krauss, S. Schumann, F. Siegert, QCD matrix elements and truncated showers, JHEP 05 (2009) 053. arXiv:0903.1219, doi:10.1088/1126-6708/2009/05/053.

[56] S. "Höche, F. Krauss, M. Schonherr, F. Siegert, QCD matrix elements + parton showers: The NLO case, JHEP 04 (2013) 027. arXiv:1207.5030, doi:10.1007/JHEP04(2013)027.

[57] A. Andreassen, P. T. Komiske, E. M. Metodiev, B. Nachman, J. Thaler, OmniFold: A Method to Simultaneously Unfold All Observables, Phys. Rev. Lett. 124 (18) (2020) 182001. arXiv:1911.09107, doi:10.1103/PhysRevLett.124.182001.

[58] A. Andreassen, P. T. Komiske, E. M. Metodiev, B. Nachman, A. Suresh, J. Thaler, Scaffolding Simulations with Deep Learning for High-dimensional Deconvolution, in: 9th International Conference on Learning Representations, 2021. arXiv:2105.04448.

[59] M.-H. Guo, J.-X. Cai, Z.-N. Liu, T.-J. Mu, R. R. Martin, S.-M. Hu, Pct: Point cloud transformer, Computational Visual Media 7 (2021) 187–199.

[60] V. Mikuni, F. Canelli, Point cloud transformers applied to collider physics, Mach. Learn. Sci. Tech. 2 (3) (2021) 035027. arXiv:2102.05073, doi:10.1088/2632-2153/ac07f6.

[61] Perlmutter system, https://docs.nersc.gov/systems/perlmutter/system_details/, accessed: 2022-05-04.

[62] A. Sergeev, M. D. Balso, Horovod: fast and easy distributed deep learning in TensorFlow, arXiv preprint arXiv:1802.05799 (2018).

[63] R. Kogler, Measurement of jet production in deep-inelastic ep scattering at hera, https://www-h1.desy.de/psfiles/theses/h1th-590.pdf (Feb 2011).

[64] V. Andreev, et al., Measurement of multijet production in ep collisions at high Q^2 and determination of the strong coupling α_s, Eur. Phys. J. C 75 (2) (2015) 65. arXiv:1406.4709, doi:10.1140/epjc/s10052-014-3223-6.

[65] F. D. Aaron, et al., Measurement of $D^{*\pm}$ Meson Production and Determination of $F_2^{c\bar{c}}$ at low Q^2 in Deep-Inelastic Scattering at HERA, Eur. Phys. J. C 71 (2011) 1769, [Erratum: Eur.Phys.J.C 72, 2252 (2012)]. arXiv:1106.1028, doi:10.1140/epjc/s10052-011-1769-0.

[66] F. D. Aaron, et al., Inclusive Deep Inelastic Scattering at High Q^2 with Longitudinally Polarised Lepton Beams at HERA, JHEP 09 (2012) 061. arXiv:1206.7007, doi:10.1007/JHEP09(2012)061.

[67] B. Efron, Bootstrap Methods: Another Look at the Jackknife, Annals Statist. 7 (1) (1979) 1–26. doi:10.1214/aos/1176344552.